RSC Advances

ROYAL SOCIETY OF CHEMISTRY

www.rsc.org/advances

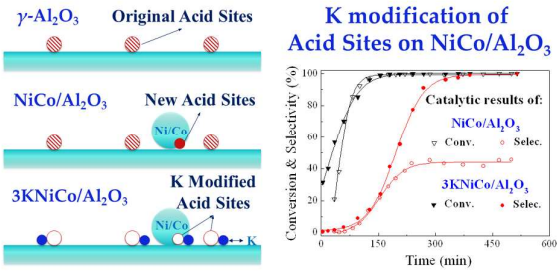

K modification suppressed both the original and the newly formed acid sites on the $NiCo/Al_2O_3$ catalyst, which were responsible for the condensation reactions in the IPN hydrogenation network.

Isophthalonitrile (IPN) Hydrogenation over K modified Ni-Co Supported Catalysts: Catalyst Characterization and Performance Evaluation

Chang Liu, Tiefeng Wang*

Beijing Key Laboratory of Green Reaction Engineering and Technology

Department of Chemical Engineering, Tsinghua University, Beijing, 100084, China

**Corresponding author: 86-10-62794132, wangtf@tsinghua.edu.cn*

Abstract

The hydrogenation of Isophthalonitrile (IPN) to meta-xylylenediamine (*m*-XDA) is usually catalyzed by the Raney or supported Ni based catalysts in the presence of basic additive. Although the supported catalysts are safer than the Raney Ni catalysts, they have lower selectivity to *m*-XDA. This work revealed that the acid sites of $NiCo/Al_2O_3$ were responsible for the condensation reactions between amines and imines, which were the dominant side reactions. Besides the original acid sites on γ-Al_2O_3, the loading of Ni-Co introduced new acid sites, which had a greater contribution to the condensation reactions. The K modification significantly enhanced the selectivity to *m*-XDA by reducing the two kinds of acid sites. Due to the formation mechanism of new acid sites and the K modification mechanism on these sites, both the K loading and K impregnation sequence affected the catalytic performance. When 3.0 wt% K was introduced to $NiCo/Al_2O_3$ by co-impregnation ($3KNiCo/Al_2O_3$), the catalyst acidity decreased by 82%, and the selectivity to *m*-XDA increased from 45.5% to 99.9%. The superiority of the optimized catalyst $3KNiCo/Al_2O_3$ was also confirmed when no basic additive was used.

Keywords: IPN hydrogenation, K modification, Ni-Co supported catalyst, catalyst acidity

1. Introduction

The hydrogenation of nitriles is an important industrial process to produce primary amines[1-3], which are widely used as solvents, pharmaceuticals, disinfectants, rubber stabilizers, textile additives, and chemical intermediates[4, 5]. For example, meta-xylylenediamine (*m*-XDA), an ideal curing agent of epoxy[5, 6], is produced by catalytic hydrogenation of isophthalonitrile (IPN)[5-7].

In the industrial process of IPN hydrogenation, Raney Ni[3, 8] is the most widely used catalyst and has a high selectivity to *m*-XDA. Other Raney catalysts, such as the Raney Co[9, 10] and modified Raney catalysts[5], are also used. However, due to the skeleton structures[11], the Raney catalysts have low mechanical strength, leading to a high catalyst consumption. Besides, they are flammable when exposed in air, therefore they should be used very carefully to ensure safety. In the hydrogenation of IPN, the catalysts deactivate due to the condensation reactions, which requires the regeneration ability of the catalysts. However, the Raney catalysts cannot be regenerated by the common combustion method due to their flammability. In recent years, more attentions have been paid to the supported catalysts for nitrile hydrogenation reactions, with transition metals from the VIII group as the active components, including precious metals of Pd, Pt and Ru[1, 12-14], and nonprecious metals such as Ni and Co[1, 6, 15-17]. Among all the active metals, Ni and Co have the highest selectivity to primary amines[17], and the Ni and Co based catalysts are more economical for industrial use. In the supported multimetallic catalysts, the synergy effects between the metal components contribute to the enhanced catalytic performance, and the supports provide good mechanical strength. For the supported Ni based catalysts, the metal loadings had a significant influence on the product distribution, and a low selectivity to primary amines was obtained at low metal loadings. To suppress the side reactions and get a high selectivity (> 90%) to

primary amines, a high Ni loading (> 10 wt%) of nickel-based supported catalysts was used[1, 6, 15-17].

The mechanism of nitrile hydrogenation has been studied by many researchers[1, 2, 9, 18]. According to these studies, the mechanism of IPN hydrogenation is shown in Scheme 1. In the sequential hydrogenation of C≡N, the highly reactive intermediate imine is formed, which has been confirmed by the attenuated total reflection infra-red (ATR-IR) spectra[19]. In addition to further hydrogenation to primary amines, the condensation reactions between imines and amines occur as dominant side reactions, which form higher amines and other oligomers[1, 12], and lead to catalyst deactivation. By optimizing the catalyst composition and reaction conditions, and using basic additive, these side reactions can be effectively suppressed[4, 5, 17, 20, 21].

In the reaction network of IPN hydrogenation, the different reactions are supposed to be catalyzed by different sites on the catalysts. A bifunctional mechanism proposed by Verhaak[22] revealed that the acid sites on the catalyst were responsible for the side reactions, which was confirmed by the gas-phase hydrogenation of acetonitrile over Ni[22-25] and Pt[26] supported catalysts, gas-phase hydrogenation of propionitrile[27, 28], and liquid-phase hydrogenation of lauronitrile[27, 28]. However, the underlying mechanism of the generation and effect of the acid sites is still not well understood and there are contradictory results on the effect of support acid-base property on the catalytic performance[13, 29]. For example, Rode et al.[29] reported that in the hydrogenation of benzonitrile and acetonitrile, the supports mainly affected the Ni dispersion and only affected the catalytic activity, while the selectivity to primary amines were almost unaffected. In conclusion, it was confirmed in the literatures that the effect of support on the catalytic performance were caused by either the acid-base property or the metal-support interaction.

Alkali doping has been widely used to modify the supported catalysts. By neutralizing the acid sites, creating new basic sites, and acting as active component or electronic factor, alkali doping can enhance the catalytic activity and selectivity, and suppress the catalyst deactivation[30]. A few studies have been reported on the alkali modification of the catalysts in nitrile hydrogenation[22,31]. In Ni/Al_2O_3 catalyzed acetonitrile gas-phase hydrogenation[22], and Ni/α-Al_2O_3 catalyzed adiponitrile liquid-phase hydrogenation[31], K modification of the catalysts effectively increased the selectivity to primary amines. However, the systematic study on the mechanism of alkali modification based on quantitative analysis is still very limited. Besides, no relevant study on the alkali modification of the catalyst in IPN hydrogenation system has been reported.

In this work, a series of K-modified Ni-Co supported catalysts were synthesized, characterized, and evaluated in IPN hydrogenation. For easier comparison between the unmodified and modified catalysts, and studying the mechanism of K modification of the acid sites, a low Ni-Co loading (5 wt% of Ni and 1.25 wt% of Co) and a weakly acidic support (γ-Al_2O_3) were adopted. The effects of K loading and impregnation sequence on the catalyst acidity and catalytic performance were systematically studied. The results showed that the K modification significantly enhanced the selectivity to *m*-XDA by reducing the catalyst acidity.

2. Experimental

2.1. Catalyst preparation

A series of K modified Ni-Co supported catalysts, *w*KNiCo/Al_2O_3 (*w* is the K loading in wt%), were synthesized by incipient wetness impregnation, using nitrates ($Ni(NO_3)_2$ $6H_2O$, 98%, $Co(NO_3)_2$ $6H_2O$, 98.0%, KNO_3, 99.0%, Alfa Aesar) as the metallic precursors, and γ-Al_2O_3 as the support (Alfa Aesar, grinded to 40–80 mesh). The Ni and Co loadings were 5.0 and 1.25 wt%,

respectively, and the K loading varied from 0.1 to 5.0 wt% (w= 0.1–5.0). Co-impregnation was used for all K loadings. The unmodified $NiCo/Al_2O_3$ catalyst was prepared similarly, except that no K was impregnated. To study the effects of impregnation sequence, the sequential impregnation method was also used to prepare the catalysts with 1.0 and 3.0 wt% K loadings, which were denoted as wK-$NiCo/Al_2O_3$ and NiCo-wK/Al_2O_3 (w= 1, 3) according to the impregnation sequence. For wK-$NiCo/Al_2O_3$, K was impregnated before Ni-Co, and for NiCo-wK/Al_2O_3, K was impregnated after Ni-Co.

The impregnated samples were aged overnight at room temperature after an ultrasonic treatment for 1 h. The catalyst precursors were then dried in air at 80 ^{o}C for 6 h, heated to 100 ^{o}C in 20 min and kept for another 20 min to remove the physically absorbed water, and then the samples were heated to 400 ^{o}C in 30 min and calcined for 4 h. Before used in the hydrogenation reactions, the catalysts were reduced in H_2 flow (70 mL min^{-1}) at 450 ^{o}C for 5 h.

2.2. Catalyst characterization

The specific surface area, pore volume and pore size distribution of the unreduced catalysts were determined by N_2 adsorption-desorption with a Quantachrome autosorb iQ and AsiQwin instrument. The results were calculated by Brunauer-Emmett-Teller (BET) and Barrett-Joyner-Halenda (BJH) methods.

The CO-uptake of the catalysts was determined by CO chemisorption on a Quantachrome ChemBET Pulsar TPR/TPD instrument. Before the measurement, the catalysts were reduced online at 450 ^{o}C for 1 h in a 5% H_2/He gas mixture at 100 mL min^{-1}, and purged by He gas flow to remove the physically absorbed H_2. The unreduced $NiCo/Al_2O_3$ and $3KNiCo/Al_2O_3$ were observed by transmission electron microscopy (TEM, JEOL2010F) in scanning mode (STEM).

Powder X-ray diffraction (XRD) tests of the unreduced catalysts were performed using a Bruker D8 Advance powder X-ray diffractometer (40 kV, 40 mA) with a Cu K_α radiation source and a Ni filter in the 2θ range 5–90 ^{o}.

The acidities of the reduced catalysts were measured by ammonia temperature-programmed desorption (NH_3-TPD) using a Quantachrome ChemBET Pulsar TPR/TPD instrument. Before the TPD analysis, the catalyst of 200 mg was reduced online for 1 h at 450 ^{o}C. After the reduction, the catalyst sample was cooled to 80 ^{o}C, exposed in a 5% NH_3/He gas mixture for 45 min, and purged by He gas flow to remove the physically adsorbed NH_3, until the signal of thermal conductivity detector (TCD) reached a constant level. Finally, the NH_3-TPD test was conducted by heating to 600 ^{o}C with the signal of NH_3 desorption recorded by TCD.

Temperature programmed reduction (TPR) was also conducted on the Quantachrome ChemBET Pulsar TPR/TPD instrument. The TPR tests were carried out in a flow of a 5% H_2/He mixture at 100 mL min^{-1} at a heating rate of 10 ^{o}C min^{-1}. The H_2 consumption was detected and recorded by TCD.

A Thermal Scientific ESCALAB 250Xi was used to examine the oxidation state of the surface atoms of the unreduced NiCo/Al_2O_3 and 3KNiCo/Al_2O_3 catalysts. The Al-K_α X-ray source was used.

2.3. Catalytic reaction

The hydrogenation reactions of IPN were carried out in a stainless steel autoclave (Weihai Chemical Machinery Co., Ltd., 250 mL) equipped with an automatic temperature control system and a magnetically driven impeller. A continuous H_2 flow was controlled by a mass flow meter, and the operating pressure was controlled by a back-pressure valve at the outlet. The

hydrogenation conditions were set as follows: 80 °C, 6.0 MPa, stirring speed of 800 rpm, and H_2 flow rate of 190 mL min^{-1}. Preliminary experiments showed that at these conditions the influence of external and internal diffusion was eliminated.

In a typical experiment, 2.9 g of IPN (98%, J&K Chemical), 20 mL of methanol (> 99.5%, Beijing Chemical Works) and 80 mL of toluene (> 99.5%, Beijing Modern Oriental Fine Chemistry Co., Ltd.) were added into the reactor, and 0.086 g of NaOH (> 96.0%, Beijing Chemical Works) was used as basic additive. Additional experiments without basic additive were carried out for comparison. For each experiment, 5.0 g of the pre-reduced and passivated catalyst was transferred to the solvent in the autoclave. The system was purged with H_2 gas flow for 30 min under 300 rpm stirring. The reactor was heated to the reaction temperature (80 °C) under 0.3 MPa, and was then pressurized to 6.0 MPa within 5 min. At the same time, the H_2 flow rate and stirring speed were set to the specified values. During the above operations, the heating process was conducted at a relatively low pressure so that only a small amount of IPN was converted during this period, and the time when the pressure reached to 6.0 MPa could be considered as zero time of the reaction.

The products were sampled online with a time interval of 10 min and were analyzed by gas chromatography (GC 7900II, Techcomp Instrument Company) equipped with a DB-1MS UI capillary column (30m × 0.25mm × 0.25um, Agilent) and an FID detector.

The conversion of IPN and the selectivity to m-XDA were calculated as:

$$\text{IPN conversion} = \frac{\text{moles of converted IPN}}{\text{moles of IPN feedstock}} \times 100\% \quad (1)$$

$$\text{Product selectivity} = \frac{\text{moles of carbon in a defined product}}{\text{moles of carbon in converted IPN}} \times 100\% \quad (2)$$

Besides *m*-XDA and unconverted IPN, the liquid sample also contained higher amines and other oligomers, which could not be detected by gas chromatography. Therefore, the species in the final liquid samples were analyzed by mass spectrometry (MS, instrument model: Q Exactive) to identify the heavier species.

3. Results and discussion

3.1. Catalyst characterization

3.1.1. BET surface area

The physical properties of unreduced *w*KNiCo/Al_2O_3, NiCo/Al_2O_3 and bare γ-Al_2O_3 (calcined before analysis) are listed in Table 1. The bare γ-Al_2O_3 had a surface area of 221 $m^2 g^{-1}$, and a pore volume of 0.63 $cm^3 g^{-1}$, which decreased after the introduction of Ni-Co. At a K loading not higher than 3.0 wt%, the surface area and pore volume of *w*KNiCo/Al_2O_3 were nearly the same as that of the unmodified NiCo/Al_2O_3. However, when the K loading increased to 5.0 wt%, the surface area decreased from 209 to 179 $m^2 g^{-1}$, and the pore volume decreased from 0.57 to 0.47 $cm^3 g^{-1}$, compared with NiCo/Al_2O_3. The loading of K and Ni-Co had little effects on the pore size distribution (Fig. S1) and average pore diameter, which kept unchanged within 7.88–7.92 nm. Additionally, the impregnation sequence showed negligible effects on the physical properties of *w*KNiCo/Al_2O_3 (*w*= 1, 3).

From theoretical calculations, the coverage of K on the support surface would reach 100% at the K loading of ≈ 5 wt%. In actual situations, however, the layer thickening and aggregation would occur at lower loading due to the non-uniform loading, and result in multilayers of K and blocking of the pore structures. Correlating to the theoretical calculation results, the above BET results could be attributed to the relatively uniform dispersion of K on the support at K loadings

not higher than 3.0 wt%, which barely blocked the pore structures. Similar BET results were also reported in the literatures for Ni/SiO_2, Co/SiO_2 and alkali-doped (Li, Rb) Au/Al_2O_3[17, 32]. At the K loading of 5.0 wt%, the effects of K loading on the physical properties were significant, and the decrease in the BET surface area and pore volume was due to the enhanced generation of multilayers of K and the blocking of the pore structures.

3.1.2. XRD

The XRD profiles of bare γ-Al_2O_3, $NiCo/Al_2O_3$, and *w*$KNiCo/Al_2O_3$ catalysts (unreduced) are shown in Fig. 1. Confirmed by the XRD analysis of $NiCo/Al_2O_3$ with higher loadings (Fig. S2), NiO, Co_3O_4, $NiCo_2O_4$ and the Ni/Co aluminates are the main phases, consistent with the literatures[33, 34]. In this study, the XRD profile of γ-Al_2O_3 showed little changes after the loading of either Ni-Co or Ni-Co-K, without distinguishable characteristic peaks of Ni/Co oxides and aluminates. Considering the low contents of Ni, Co and K, and the similar peak locations of Ni/Co oxides and γ-Al_2O_3, this result could be attributed to the overlapped peaks of Ni/Co oxides and γ-Al_2O_3. The formation of ill-crystallized surface compound such as Ni aluminate[35, 36] and Co aluminate[34] was also a possible reason. According to De Bokx[36], in the calcined Ni/γ-Al_2O_3 catalysts with low Ni content, Ni was present exclusively as a "surface aluminate", while a separate NiO phase was detected only at higher Ni loadings.

3.1.3. CO chemisorption and TEM results

The CO chemisorption results showed that the CO-uptake of $3KNiCo/Al_2O_3$ (337 $\mu L\ g^{-1}$) was similar to that of $NiCo/Al_2O_3$ (322 $\mu L\ g^{-1}$), both indicating low metal dispersions (1.42% and 1.35%, respectively, assuming a chemisorption stoichiometric factor of 1.0 for both Ni and Co). Fig. 2 shows the HAADF TEM images of the unreduced $NiCo/Al_2O_3$ and $3KNiCo/Al_2O_3$. The

HAADF images indicated a relatively more uniform dispersion of Ni/Co oxides on 3KNiCo/Al_2O_3, on which the Ni/Co oxide particles were hard to detect. While on NiCo/Al_2O_3, the Ni/Co oxide particles were detected and identified by the EDS surface scanning results (Fig. S3), with the particle size distributed around 10 nm.

3.1.4. Catalyst acidity

The NH_3-TPD curves of bare γ-Al_2O_3, and reduced *w*KNiCo/Al_2O_3 and NiCo/Al_2O_3 catalysts are shown in Fig. 3. All the samples showed a broad desorption peak in the temperature range of 100–500 ^oC, which made it difficult to distinguish the weak, medium and strong acid sites. In this work, the total acidity of each catalyst was calculated from the desorbed amount of NH_3, and is summarized in Table 1. After the introduction of Ni-Co, the total acidity increased from 0.180 to 0.474 mmol NH_3 g^{-1}. Similar results were reported in the literatures[35, 37-40]. The enhanced acidity was caused by the formation of $NiAl_2O_4$ and $CoAl_2O_4$[30, 36, 37], in which the surface net positive charge is higher than that in pure γ-Al_2O_3. In our experiments, similar results were also found on the NiCo/SiO_2 catalyst (Table S1), indicating that the new acid sites were formed even on a much weaker-acidic support. Therefore, the acid sites could not be eliminated by using a support having much weaker acidity, such as SiO_2. The modification of the supported catalysts was necessary to increase the selectivity to *m*-XDA.

By K modification, the catalyst acidity was well modulated. With the K loading increasing from 0 to 5.0 wt%, the catalyst acidity significantly reduced from 0.474 to 0.078 mmol NH_3 g^{-1}. This could be attributed to the neutralization and blocking of the acid sites by K modification[30]. Besides the K loading, the impregnation sequence of K also had an effect on the catalyst acidity. At a certain K loading (*w*= 1, 3), the pre-impregnated (*w*K-NiCo/Al_2O_3) and post-impregnated

(NiCo-*w*K/Al_2O_3) catalysts showed similar acidity, which were higher than that of the co-impregnated catalyst (*w*KNiCo/Al_2O_3). For instance, at 3.0 wt% K loading, the catalysts prepared by sequential impregnation (3K-NiCo/Al_2O_3 and NiCo-3K/Al_2O_3) had 17.6% higher acidity than the co-impregnated catalyst 3KNiCo/Al_2O_3 (0.098, 0.100 and 0.085 NH_3 g^{-1}, respectively). For the catalysts modified by 1.0 wt% K, the effect of impregnation sequence was weaker than that for thier 3 wt% K modified counterparts.

3.1.5. H_2-TPR results

The H_2-TPR profiles of *w*KNiCo/Al_2O_3 and NiCo/Al_2O_3 are shown in Fig. 4. The results of 5.0 wt% Co/Al_2O_3 and 5.0 wt% Ni/Al_2O_3 were included for comparison. In the monometallic catalysts, the reduction of Ni oxide had two peaks at 450 ^oC and 700 ^oC, and the reduction peak of Co oxide appeared at 475 ^oC. For the unmodified NiCo/Al_2O_3 catalyst, the reduction of Ni and Co oxides had two peaks at around 370 ^oC and 670 ^oC, indicating enhanced reducibility compared with the monometallic catalysts. In the range of $0 \leq w \leq 1.0$, the reduction peaks of *w*KNiCo/Al_2O_3 shifted to lower temperatures with increasing K loading, indicating that the reducibility of Ni/Co oxides was enhanced by K modification. When the K loading increased to 3.0 wt%, the reduction peak temperature was similar to that of 1KNiCo/Al_2O_3. For 5KNiCo/Al_2O_3, however, the TPR peak shifted backward to the higher temperature region. In addition, the TPR peak area increased with increasing K loading. Considering that the $NiAl_2O_4$ and $CoAl_2O_4$ were less reducible than Ni/Co oxides[6], the shift of TPR peak and the increased peak area suggested that the K modification decreased the amount of $NiAl_2O_4$ and $CoAl_2O_4$ and increased that of Ni/Co oxides. The reduction of Ni/Co oxides and the exposure of metallic Ni and Co were facilitated by K modification with K loadings below 3.0 wt%.

The H_2-TPR results were instructive for the determination of reduction conditions of the catalysts. As reported by Verhaak et al.[22], the acidic nickel hydrosilicate was responsible for the acid-base properties of Ni/SiO_2. The acidity and catalytic performance in acetonitrile hydrogenation of the Ni/SiO_2 catalyst highly depended on the reduction temperature and time. With increasing reduction temperature and time, the degree of reduction of the catalyst was enhanced, leading to lower acidity. According to the literature[22] and the H_2-TPR results in this work, a high reduction temperature (450 ^{o}C) and a moderate reduction time (4 h) were used.

3.1.6. XPS

The Ni2*p* and Co2*p* binding energies (Ni2$p_{3/2}$ BE and Co2$p_{3/2}$ BE) of the unreduced $NiCo/Al_2O_3$, $3KNiCo/Al_2O_3$, $3K\text{-}NiCo/Al_2O_3$ and $NiCo\text{-}3K/Al_2O_3$ catalysts were analyzed by XPS, and the results were listed in Table 2. The Ni2$p_{3/2}$, Co2$p_{3/2}$ and K2$p_{3/2}$ BEs were around 855, 781 and 293 eV, respectively, which belonged to their oxidation states[41,42]. The Ni2*p* and Co2*p* BEs decreased after K modification. Compared with $NiCo/Al_2O_3$, the Ni2$p_{3/2}$ BE of $3KNiCo/Al_2O_3$ decreased from 855.78 to 855.50 eV, and the Co2$p_{3/2}$ BE decreased from 781.18 to 780.89 eV, indicating higher electron densities of the Ni and Co surface atoms in $3KNiCo/Al_2O_3$. According to the literature[43], the electropositive K atoms would donate extra electron density to the Ni surface atoms in the Ni supported catalysts. It was also found that the Ni2$p_{3/2}$ and Co2$p_{3/2}$ BEs of $3KNiCo/Al_2O_3$ were lower than that of $3K\text{-}NiCo/Al_2O_3$ and $NiCo\text{-}3K/Al_2O_3$. The electronic effect depended on the loading sequence of K, and was most significant with co-impregnation of K.

The introduction of K also affected the surface concentration of Ni-Co. As shown in Table 2, the Ni-Co/Al surface atomic ratio decreased from 0.100 on $NiCo/Al_2O_3$ to 0.074–0.083 on K

modified catalyst due to the existence of K surface atoms. The Ni-Co and K surface composition was almost independent of the loading sequence of K, except that the surface K concentration of 3K-NiCo/Al_2O_3 was significantly lower than that of 3KNiCo/Al_2O_3 and NiCo-3K/Al_2O_3, because K was covered by the subsequent loading of Ni and Co.

3.2. Catalytic performance

3.2.1. Effects of K loading

The K modified catalysts *w*KNiCo/Al_2O_3 and the unmodified catalyst NiCo/Al_2O_3 were evaluated in the IPN hydrogenation reaction under the same conditions in the presence of 0.086 g NaOH as basic additive. The rate constants (k_r) of the IPN hydrogenation reaction and selectivity to *m*-XDA over *w*KNiCo/Al_2O_3 and NiCo/Al_2O_3 are listed in Table 1. The reaction order (p) and the rate constant (k_r) of IPN hydrogenation were calculated by fitting the experiment data of IPN concentration as a function of reaction time with a power rate law, as shown in Eq. (3), and the data in the first 100 min were used.

$$\frac{dC_{IPN}}{dt} = -k_r C_{IPN}^{p} \quad (3)$$

Using a 0.8-order reaction model, the rate constant k_r could be calculated from the regression results. With the increase of K loading, k_r exhibited a decreasing trend. With the K loading below 1.0 wt%, the value of k_r was in the range of 2.0×10^{-2}–2.3×10^{-2} $mol^{0.2}$ $L^{-0.2}$ min^{-1}. With a further increase of the K loading, k_r gradually decreased. For 2KNiCo/Al_2O_3 and 3KNiCo/Al_2O_3, the activity decreased by about 43% compared with the unmodified catalyst (k_r decreased from 2.1×10^{-2} to 1.3×10^{-2} and 1.1×10^{-2} $mol^{0.2}$ $L^{-0.2}$ min^{-1}). With a further increase of the K loading to 5.0 wt%, k_r significantly decreased to 0.2×10^{-2} $mol^{0.2}$ $L^{-0.2}$ min^{-1}. Meanwhile, the selectivity to *m*-XDA was much enhanced. The selectivity to *m*-XDA increased from 45.5% over NiCo/Al_2O_3 to nearly

100% over 3KNiCo/Al_2O_3.

For each experiment, the species in the final liquid samples were identified by MS to verify the byproducts, as shown in Fig. S4. The MS measurement conditions were mild so that degradation of the oligomers was avoided. In the MS spectra, the peaks at m/z of 137 and 120 belonged to the protonated and deammoniated *m*-XDA, respectively; while those around m/z of 255 and 374 were the peaks of dimerization and trimerization products, respectively. The MS results showed that the enhanced formation of higher amines was responsible for the decreased selectivity to *m*-XDA. At a K loading of 3.0 wt%, only a trace amount of higher amines were detected, confirming that the condensation reactions between imines and amines were effectively suppressed by K modification.

To further analyze the effect of K modification, the selectivity to *m*-XDA was plotted as a function of the acidity density of the catalyst, as shown in Fig. 5. The results showed that the selectivity to *m*-XDA strongly depended on the catalyst acidity. The increased selectivity to *m*-XDA over the K modified catalysts could be attributed to the weakened adsorption of imines on the catalytic sites due to the suppressed acidity, which was the result from the blocking of the acid sites and the suppressed formation of $NiAl_2O_4$ and $CoAl_2O_4$ by K modification. The enhanced selectivity to *m*-XDA was also attributed to the increased electron density of Ni and Co donated by K, which favored the adsorption of nitriles by enhancing the N-metal bond, thus weakened the strength of C≡N or C=N and facilitated the attack of adsorbed Hatom to the Cto or C=N groups in the IPN hydrogenation reaction[16]. The electron-enriched Ni/Co sites also reduced the condensation reactions by inhibiting the adsorption of *m*-XDA, as reported in similar reactions of acetonitrile hydrogenation catalyzed by amorphous NiB and CoB alloys[44]. The activity decrease in the K

modified catalysts was caused by change in the morphology or component of the metal particles. Verhaak et al.[22] reported that with K modification, less active Ni crystal planes were exposed on the surface, leading to the decrease in acetonitrile hydrogenation activity of Ni/Al_2O_3. The formation of inactive alkali metal aluminates was also a possible reason[45]. In this work, the decreased activity was mainly caused by the altered surface Ni-Co composition of the catalyst. As shown by the XPS results, the Ni-Co surface density of the K modified catalysts was lower than that of $NiCo/Al_2O_3$, which was responsible for the decreased activity.

3.2.2. Effects of impregnation sequence

The effects of the impregnation sequence were studied with the catalysts modified by 1.0 and 3.0 wt% K, and the results were listed in Table 1. Overall, the effects of the impregnation sequence were more significant with 3.0 wt% K than with 1.0 wt% K. For the 1.0 wt% K modified catalysts, the reaction rate constants of both 1K-$NiCo/Al_2O_3$ and NiCo-1K/Al_2O_3 were similar to that of 1K$NiCo/Al_2O_3$, while the selectivity to *m*-XDA decreased only slightly from 62.4% over 1K$NiCo/Al_2O_3$ to 58.6% over 1K-$NiCo/Al_2O_3$ and 59.8% over NiCo-1K/Al_2O_3. For the 3.0 wt% K modified catalysts, the effects of impregnation sequence were more significant. The rate constant k_r increased from 1.1×10^{-2} $mol^{0.2}$ $L^{-0.2}$ min^{-1} over 3K$NiCo/Al_2O_3$ to 2.2×10^{-2} $mol^{0.2}$ $L^{-0.2}$ min^{-1} over 3K-$NiCo/Al_2O_3$ and 1.6×10^{-2} $mol^{0.2}$ $L^{-0.2}$ min^{-1} over NiCo-3K/Al_2O_3, while the selectivity to *m*-XDA decreased from 99.9% to 79.7% and 85.4%. To better compare the optimized catalyst 3K$NiCo/Al_2O_3$ with the unmodified $NiCo/Al_2O_3$, the conversion of IPN and the selectivity to *m*-XDA were plotted as a function of reaction time, as shown in Fig. 6 (a). The results of $NiCo/Al_2O_3$ and 3K$NiCo/Al_2O_3$ had similar profiles, indicating that the reaction pathways were independent of the K modification. In the sequential hydrogenation, IPN was first

converted to *m*-CBA, as shown in Scheme 1. The second hydrogenation step, namely the *m*-CBA hydrogenation step, was slower than the first hydrogenation step, leading to a delay in the curve of the *m*-XDA selectivity compared to that of the IPN conversion. The results showed that 3KNiCo/Al_2O_3 had 54.4% higher selectivity to *m*-XDA, with the activity decreased by 47.6% compared to NiCo/Al_2O_3.

As reported in the literature[37, 38], bare γ-Al_2O_3 had a certain amount of original acidity. In this work, it was revealed that newly formed acid sites were generated on NiCo/Al_2O_3 due to the formation of $NiAl_2O_4$ and $CoAl_2O_4$. Both the original and the newly formed acid sites could be covered by K modification, because both the pre- and post- impregnation of K reduced the catalyst acidity. The newly formed acid sites could be suppressed by K in the process of their formation, thus a more effective modification of acid sites was achieved by co-impregnation of K. Tennison[46] proposed that there were three possible locations of the alkali metals on the alkali modified supported metallic catalysts: (1) within the crystallites of metal, possibly as a complex; (2) in contact with the support and metal simultaneously (the "hot ring" promotion); (3) on the surface of the metal or support. In this work, reasonable explanations of the modification effects of K to the NiCo/Al_2O_3 catalyst were as follows:

(1) The neutralization effect of K acted on both the original and newly formed acid sites, by adsorbing on the surface of γ-Al_2O_3 and the frontiers between Ni-Co and γ-Al_2O_3, leading to the reduced acidity of the *w*KNiCo/Al_2O_3 catalysts;

(2) By the "hot ring" promotion, the modification by K reduced the formation of $NiAl_2O_4$ and $CoAl_2O_4$ spinel, and suppressed the generation of new acid sites.

The discrimination between the two kinds of acid sites was reflected in the catalytic

performances. In spite of their similar acidity amounts, the NiCo-*w*K/Al_2O_3 catalysts were more selective to *m*-XDA than *w*K-NiCo/Al_2O_3, especially for the 3.0 wt% K modified catalysts. These results indicated that the newly formed acid sites had greater contributions to the side reactions, and the K modification had different effects on the two kinds of acid sites. For the co-impregnated catalysts *w*KNiCo/Al_2O_3, the newly formed acid sites were most effectively eliminated. For the *w*K-NiCo/Al_2O_3 catalysts, the K modification mainly affected the original acid sites on the γ-Al_2O_3 support; while for the NiCo-*w*K/Al_2O_3 catalysts, the newly formed acid sites had been generated before the K modification, and the subsequent loading of K could only eliminate part of these acid sites. Among all the catalysts, 3KNiCo/Al_2O_3 prepared by co-impregnation had the most effective suppression of the acidity by K modification, and had the highest selectivity to *m*-XDA with only a slight decrease in the activity. In our research, a series of *w*KNiCo/SiO_2 catalysts with different K loadings were also studied (Table S1), the results of which further confirmed the generation mechanism and the effect of the acid sites.

3.2.3. Catalytic performances without basic additives

Basic additive is used in the industrial process of IPN hydrogenation to suppress the side reactions. However, this cause troubles in the subsequent separation process due to the precipitation of basic additive at high temperatures. Therefore, additional reaction experiments were carried out without basic additive. Fig. 6(b) shows the conversion of IPN and selectivity to *m*-XDA over two typical catalysts, namely NiCo/Al_2O_3 and 3KNiCo/Al_2O_3, evaluated without basic additive. For each catalyst, the selectivity to *m*-XDA was about 14% lower without basic additive, with a slight increase in catalytic activity. For the NiCo/Al_2O_3 catalyst, the selectivity to *m*-XDA decreased from 45.5% with the addition of NaOH to 31.4% without NaOH. For the

3KNiCo/Al_2O_3 catalyst, the selectivity to *m*-XDA decreased from 99.9% to 85.7%. These results show that the basic additive effectively enhanced the selectivity to *m*-XDA. The 3KNiCo/Al_2O_3 catalyst had a high selectivity to *m*-XDA even without basic additive, showing that K modification was very effective to suppress the side reactions and it was also promising to avoid the use of basic additive by further catalyst optimization. The recycling of the optimal catalyst 3KNiCo/Al_2O_3 has been conducted with and without basic additives. At the conditions with NaOH as basic additives, the catalytic performance was almost unchanged after repeatedly used for 5 times in reaction, with the *m*-XDA selectivity kept around 99.5–99.9%. To confirm the recyclability and regeneration ability, 3KNiCo/Al_2O_3 was evaluated without basic additives, and the results were shown in Table 3. After 3 rounds of reaction, the catalytic activity was little changed, while the *m*-XDA selectivity decreased to 73.2%. By calcination at 450 ^{o}C for 4 h, the catalyst could be well regenerated, and the regenerated catalyst had 87.4% selectivity to *m*-XDA, which was comparable to that of the fresh catalyst.

The results confirmed that the decrease of the catalyst selectivity was more significant at lower *m*-XDA selectivity, caused by the condensation reactions. The 3KNiCo/Al_2O_3 catalyst had acceptable recyclability and excellent regeneration ability even at severe reaction conditions.

4. Conclusions

The K modified Ni-Co supported catalysts, *w*KNiCo/Al_2O_3, were synthesized and evaluated for the IPN hydrogenation reaction. By K modification, the physical morphology of *w*KNiCo/Al_2O_3 was almost unchanged and the reducibility of Ni/Co oxides was enhanced except for 5KNiCo/Al_2O_3. The K modification decreased the total amount of the catalyst acidity and significantly enhanced the selectivity to *m*-XDA, with only a slight decrease in activity. Both the

K loading and impregnation sequence had effects on the catalyst acidity and selectivity, indicating the original acid sites on the support and the newly formed acid sites generated from Ni-Co introduction had different effects on the reactions, and the newly formed acid sites had a greater contribution to the side reactions. Among all the catalysts, the $3KNiCo/Al_2O_3$ catalyst prepared by co-impregnation had the best performance, having a 99.9% selectivity to *m*-XDA in the presence of basic additives.

Acknowledgements

This work was supported by Program for New Century Excellent Talents in University of China (NCET-12-0297). This work made use of the resources of the Beijing National Center for Electron Microscopy at Tsinghua University.

References

1 Y. Huang, W. M. H. Sachtler, *Appl. Catal., A.*, 1999, **182**, 365-378.

2 C. De Bellefon, P. Fouilloux, *Catal. Rev.*, 1994, **36**, 459-506.

3 B.W. Hoffer, J.A. Moulijn, *Appl. Catal., A.*, 2009, **352**, 193-201.

4 R. K. Marella, K. S. Koppadi, Y.Jyothi, K. S. R. Rao, D. R. Burri, *New J. Chem.*, 2003, **37**, 3229.

5 S. W. Row, T. Y. Chae, K. S. Yoo, S. D. Lee, D. W. Lee, Y. Shul, *Can. J. Chem. Eng.*, 2007, **85**, 925-928.

6 T. Shi, H. Li, L.Yao, W. Ji, C. T. Au, *Appl. Catal., A.*, 2012, **425**, 68-73.

7 T. Y. Chae, S. W. Row, K. S. Yoo, S. D. Lee, D. W. Lee, *Bull. Korean Chem. Soc.*, 2006, **27**, 361-362.

8 F. Hochard, H. Jobic, J.Massardier, A. J. Renouprez, *J. Mol. Catal. A-Chem.*, 1995, **95**, 165-172.

9 P. Scharringer, T. Muller, J. Lercher, *J. Catal.*, 2008, **253**, 167-179.

10 *US Pat.*, 5 869 653, 1999.

11 B. W. Hoffer, *Tuning Raney-type and Supported Ni Catalysts for Commercial Hydrogenation Reactions*, 2003.

12 L. Hegedűs, T. Máthé, T. Kárpáti, *Appl. Catal., A.*, 2008, **349**, 40-45.

13 Y. Huang, V. Adeeva, W. M. H. Sachtler. *Appl. Catal., A.*, 2000, **196**, 73-85.

14 M.H.G. Prechtl, J.D. Scholten, J. Dupont, *J. Mol. Catal. A-Chem.*, 2009, **313**, 74-78.

15 P. Braos-García, P. Maireles-Torres, E.,Rodríguez-Castellón, A.Jiménez-López, *J. Mol. Catal. A-Chem.*, 2003, **193**, 185-196.

16 G. D. Yadav, M.R. Kharkara, *Appl. Catal., A.*, 1995, **126**, 115-123.

17 D. J. Segobia, A. F. Trasarti, C.R. Apesteguía, *Appl. Catal., A.*, 2012, **445**, 69-75.

18 J. V. Braun, G. Blessing, F. Zobel, *Berichte der deutschen chemischen Gesellschaft (A and B Series).*, 1923, **56**, 1988-2001.

19 I. Ortiz-Hernandez, C. T. Williams, *Langmuir*, 2007, **23**, 3172-3178.

20 Y. Huang, M.M.H. Sachtler, *J. Catal.*, 1999, **188**, 215-225.

21 Z. Cheng, Q. Wu, J. Li, Q. Zhu, *Catal. Today*, 1996, **30**, 147-155.

22 M. J. F. M. Verhaak, *Catal. Lett.*, 1994, **26**, 37-53.

23 A. C. Gluhoi, P. Mărginean, U. Stănescu, *Appl. Catal., A.*, 2005, **294**, 208-214.

24 A. Infantesmolina, *J. Catal.*, 2004, **225**, 479-488.

25 F. M. Cabello, D. Tichit, B. Coq, A. Vaccari, N. T. Dung, *J. Catal.*, 1997, **167**, 142-152.

26 C. Park, M. A. Keane, *J. Colloid Interface Sci.*, 2003, **266**, 183-194.

27 J. B. Branco, D. Ballivet-Tkatchenko, A. P. de Matos, *J. Mol. Catal. A-Chem.*, 2009, **307**, 37-42.

28 H. Chen, M. Xue, S. Hu, J. Shen, *Chem. Eng. J.*, 2012, **181**, 677-684.

29 C. V. Rode, M. Arai, M. Shirai, Y. Nishiyama, *Appl. Catal., A.*, 1997, **148**, 405-413.

30 W. D. Mross, *Cat. Rev.*, 1983, **25**, 591-637.

31 H. Liao, S. Liu, F. Hao, P. Liu, K. You, D. Liu, H. A. Luo, *Reac. Kinet. Mech. Cat.*, 2013, **109**, 475-488.

32 A. Gluhoi, N. Bogdanchikova, B. Nieuwenhuys, *J. Catal.*, 2005, **232**, 96-101.

33 L. Ji, J. Lin, H. C. Zeng, *J. Phys. Chem. B.*, 2000, **104**, 1783-1790.

34 D. Xu, W. Li, H. Duan, Q. Ge, H. Xu, *Catal. Lett.*, 2005, **102**, 229-235.

35 V. L. Barrio, P. L. Arias, J. F. Cambra, M. B. Güemez, *Appl. Catal., A.*, 2003, **248**, 211-225.

36 P. De Bokx, W. Wassenberg, J. Geus, *J. Catal.*, 1987, **104**, 86-98.

37 S. Benbenek, E. Fedoryńska, P. Winiarek, *React. Kinet. Catal. Lett.*, 1993, **51**, 189-195.

38 H. Lu, H. Yin, Y. Liu, T. Jiang, L. Yu, *Catal. Commun.*, 2008, **10**, 313-316.

39 K. M. Hardiman, C. G. Cooper, A. A. Adesina, *Ind. Eng. Chem. Res.*, 2004, **43**, 6006-6013.

40 A. Godelitsas, D. Charistos, E. A. A. Tsipis, *Chem. Eur. J.*, 2001, **17**, 3705-3721.

41 A. P. Grosvenor, M. C. Biesinger, R. S. C. Smart, N. S. McIntyre, *Surf. Sci.*, 2006, **600**, 1771-1779.

42 A. A. Khassin, T. M. Yurieva, V. V. Kaichev, V. I. Bukhtiyarov, A. A. Budneva, E. A. Paukshtis, V. N. Parmon, *J. Mol. Catal. A-Chem.*, 2001, **175**, 189-204.

43 C. T. Campbell, D. W. Goodman, *Surf. Sci.*, 1982, **123**, 413-426.

44 H. Li, Y. Wu, Y. Wan, J. Zhang, W. Dai, M. Qiao, *Catal. Today*, 2004, **93**, 493-503.

45 S.O. Soloviev, A. Yu. Kapran, S.N. Orlyk, E.V. Gubareni, *J. Nat. Gas Chem.*, 2011, **20**, 184-190.

46 Jennings, J. R., ed. Catalytic ammonia synthesis: fundamentals and practice, *Springer*, 1991.

Table captions

Table 1. Physical properties, acidity and reaction results of *w*KNiCo/Al_2O_3 and NiCo/Al_2O_3

Table 2. Ni/Co binding energy and atomic ratio of NiCo/Al_2O_3 and 3KNiCo/Al_2O_3

Table 3. Recycling and regeneration of 3KNiCo/Al_2O_3 without basic additives

Table 1. Physical properties, acidity and reaction results of *w*KNiCo/Al_2O_3 and NiCo/Al_2O_3

Catalyst	Physical properties			Acidity (mmol NH_3 g^{-1})	Reaction results[a]	
	S (m^2 g^{-1})	V_p (cm^3 g^{-1})	D_p (nm)		k_r (10^{-2} $mol^{0.2}$ $L^{-0.2}$ min^{-1})	$S_{m\text{-XDA}}$(%)
γ-Al_2O_3[b]	221	0.63	7.92	0.180	/	/
NiCo/Al_2O_3	209	0.57	7.88	0.474	2.1	45.5
0.1KNiCo/Al_2O_3	209	0.58	7.92	0.445	2.0	50.2
0.5KNiCo/Al_2O_3	210	0.57	7.90	0.387	2.3	50.3
1KNiCo/Al_2O_3[c]	(205) 201 (212)	(0.65) 0.56 (0.58)	(7.86) 7.90 (7.86)	(0.167) 0.155 (0.165)	(1.9) 1.7 (1.8)	(58.6) 62.4 (59.8)
2KNiCo/Al_2O_3	206	0.55	7.88	0.138	1.3	72.9
3KNiCo/Al_2O_3[c]	(211) 209 (209)	(0.55)0.53 (0.56)	(7.86) 7.90 (7.84)	(0.098) 0.085 (0.100)	(2.2) 1.1 (1.6)	(79.7) 99.9 (85.4)
5KNiCo/Al_2O_3	179	0.47	7.90	0.078	0.2	97.3

[a] Reaction conditions: 80 °C, 6.0 MPa, 5 g catalyst of 200~400 μm, 80 mL of toluene and 20 mL of methanol as solvent, 2.9 g of IPN feed, 0.086 g of NaOH, 180 mL min^{-1} H_2 gas flow, and stirring speed of 800 rpm.

[b] The γ-Al_2O_3 sample was calcined at 400 °C for 4h before analysis.

[c] The numbers in brackets on the left are results of *w*K-NiCo/Al_2O_3, and those in brackets on the right are results of NiCo-*w*K/Al_2O_3 (*w* = 1, 3).

Table 2. Ni/Co binding energy and atomic ratio of $NiCo/Al_2O_3$ and $3KNiCo/Al_2O_3$

XPS surface properties	$NiCo/Al_2O_3$	$3KNiCo/Al_2O_3$	$3K\text{-}NiCo/Al_2O_3$	$NiCo\text{-}3K/Al_2O_3$
Ni2$p_{3/2}$ BE (eV)	855.78	855.50	855.64	855.62
Co2$p_{3/2}$ BE (eV)	781.18	780.89	780.88	781.00
K2$p_{3/2}$ BE (eV)	/	293.08	293.05	293.11
Ni-Co/Al ratio	0.100	0.083	0.074	0.083
K/Al ratio	/	0.062	0.044	0.061

Table 3. Recycling and regeneration of $3KNiCo/Al_2O_3$ without basic additives

Times of Reaction	Reaction results[a]	
	k_r (10^{-2} $mol^{0.2}$ $L^{-0.2}$ min^{-1})	Selectivity to *m*-XDA (%)
1	2.4	85.7
2	2.1	86.2
3	2.2	73.2
After regeneration[b]	2.6	87.4

[a] Reaction conditions: 80 °C, 6.0 MPa, 5 g catalyst of 200~400 μm, 80 mL of toluene and 20 mL of methanol as solvent, 2.9 g of IPN feed, without basic additives, 180 mL min^{-1} H_2 gas flow, and stirring speed of 800 rpm.

[b] The used catalyst was calcined in air at 400 °C for 4 h to remove the coking, and reduced in H_2 for 5 h before reaction.

Scheme caption

Scheme 1. Reaction network of IPN hydrogenation reactions

Figure captions

Fig. 1. Standard spectra of (1) NiO, (2) Co_3O_4, and XRD results of (3) γ-Al_2O_3, (4) NiCo/Al_2O_3, (5) 0.1KNiCo/Al_2O_3, (6) 3KNiCo/Al_2O_3 and (7) 5KNiCo/Al_2O_3

Fig. 2. HAADF TEM images of (a) NiCo/Al_2O_3 and (b) 3KNiCo/Al_2O_3

Fig. 3. NH_3-TPD profiles of (0) γ-Al_2O_3, (1) NiCo/Al_2O_3, (2) 0.1KNiCo/Al_2O_3, (3) 0.5KNiCo/Al_2O_3, (4) 1KNiCo/Al_2O_3, (5) 2KNiCo/Al_2O_3, (6) 3KNiCo/Al_2O_3 and (7) 5KNiCo/Al_2O_3

Fig. 4. H_2-TPR profiles of (1) 5 wt% Ni/Al_2O_3, (2) 5 wt% Co/Al_2O_3, (3) NiCo/Al_2O_3, (4) 0.1KNiCo/Al_2O_3, (5) 1KNiCo/Al_2O_3, (6) 3KNiCo/Al_2O_3 and (7) 5KNiCo/Al_2O_3

Fig. 5. Correlation of the selectivity to *m*-XDA to the acidity of the *w*KNiCo/Al_2O_3 and NiCo/Al_2O_3 catalysts

Fig. 6. Comparison of catalytic performance of NiCo/Al_2O_3 and 3KNiCo/Al_2O_3 catalysts with or without basic additives (a) with 0.086 g NaOH as basic additive and (b) without basic additive. Other reaction conditions are the same as in Table 1.

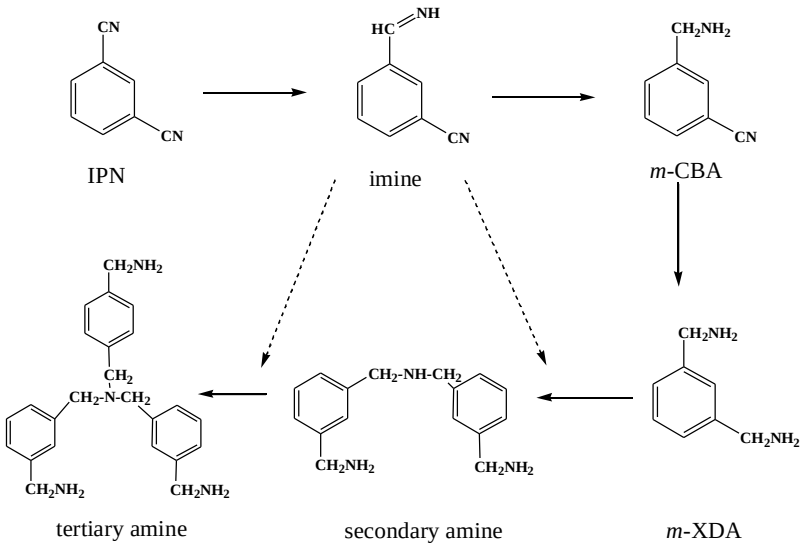

Scheme 1. Reaction network of IPN hydrogenation reactions

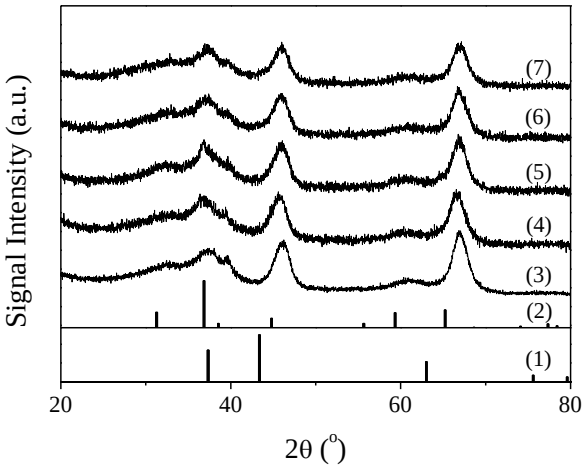

Fig. 1. Standard spectra of (1) NiO, (2) Co_3O_4, and XRD results of (3) γ-Al_2O_3, (4) NiCo/Al_2O_3, (5) 0.1KNiCo/Al_2O_3, (6) 3KNiCo/Al_2O_3 and (7) 5KNiCo/Al_2O_3

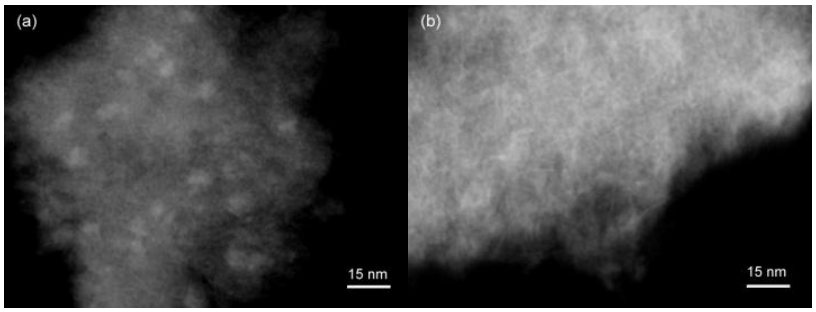

Fig. 2. HAADF TEM images of (a) NiCo/Al_2O_3 and (b) 3KNiCo/Al_2O_3

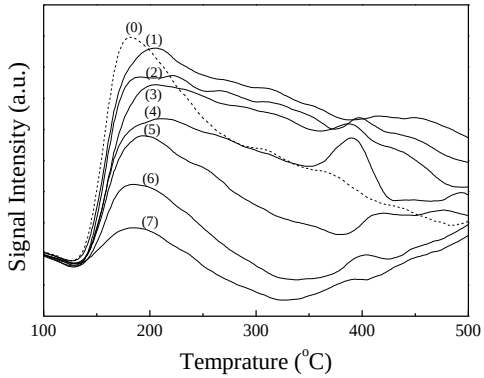

Fig. 3. NH_3-TPD profiles of (0) γ-Al_2O_3, (1) $NiCo/Al_2O_3$, (2) $0.1KNiCo/Al_2O_3$, (3) $0.5KNiCo/Al_2O_3$, (4) $1KNiCo/Al_2O_3$, (5) $2KNiCo/Al_2O_3$, (6) $3KNiCo/Al_2O_3$ and (7) $5KNiCo/Al_2O_3$

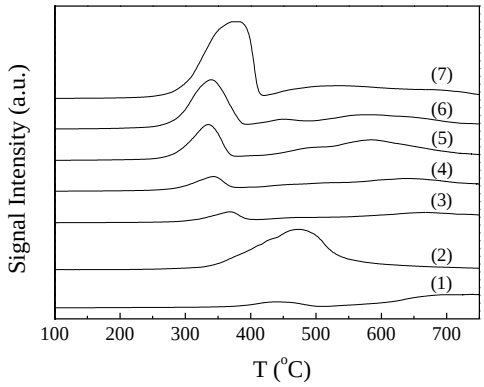

Fig. 4. H_2-TPR profiles of (1) 5 wt% Ni/Al_2O_3, (2) 5 wt% Co/Al_2O_3, (3) $NiCo/Al_2O_3$, (4) $0.1KNiCo/Al_2O_3$, (5) $1KNiCo/Al_2O_3$, (6) $3KNiCo/Al_2O_3$ and (7) $5KNiCo/Al_2O_3$

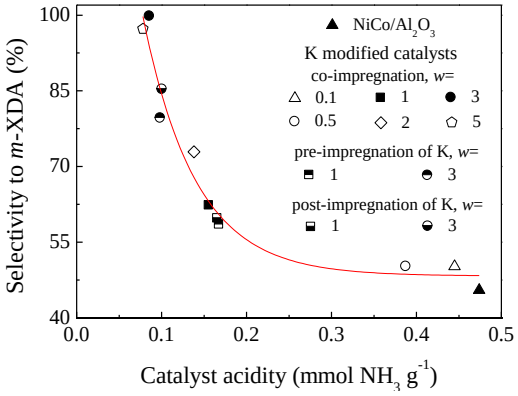

Fig. 5. Correlation of the selectivity to *m*-XDA to the acidity of the *w*KNiCo/Al_2O_3 and NiCo/Al_2O_3 catalysts

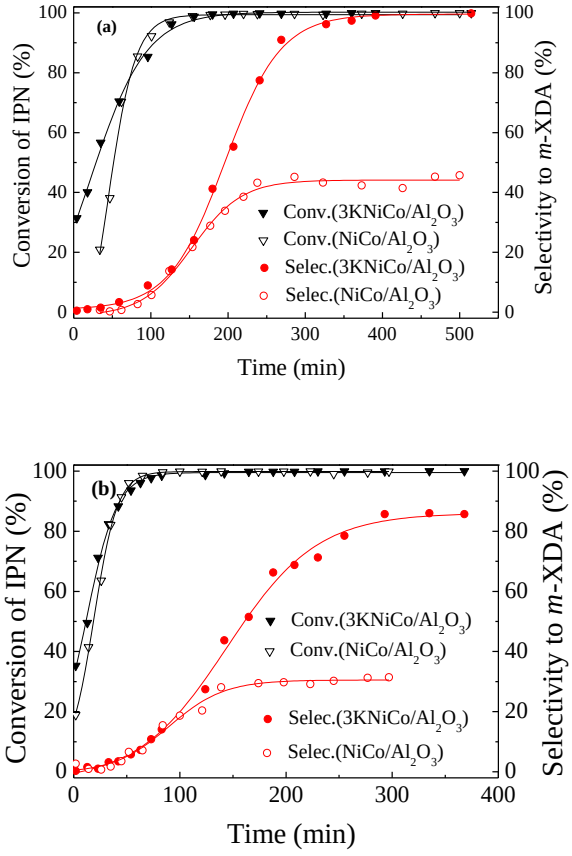

Fig. 6. Comparison of catalytic performance of NiCo/Al_2O_3 and 3KNiCo/Al_2O_3 catalysts with or without basic additives (a) with 0.086 g NaOH as basic additive and (b) without basic additive. Other reaction conditions are the same as in Table 1.